9

The Effect of Temperature on Actual Evapotranspiration based on Landsat 5 TM Satellite Imagery

Preeyaphorn Kosa
School of Civil Engineering, Institute of Engineering, Suranaree University of Technology
Thailand

1. Introduction

In the water cycle, evapotranspiration is one of the most important components, but it is one of the most difficult to measure and monitor. Evapotranspiration relates to the exchange of energy in the atmosphere, ground surface, and root zone. Some elements of calculated evapotranspiration can be measured by weather stations, while others are estimated from empirical equations. Then, the calculated evapotranspiration has some inaccuracy. To improve upon this problem, the combination of meteorological data and remote sensing observersions are an alternative evapotranspiration approach. (Hongjie et al., 2002; Kalluri et al., 2003) On the other hand, temperature is normally measured in a number of weather stations. Since temperature relates to many weather data, temperature can imply the characteristic of other weather data. For example, low temperature is included high humidity but low evaporation can be occurred in the condition of low temperature. Moreover, the variable spatial resolution is the characteristic of both actual evapotranspiration and temperature. At present, satellite image are used for studying the Earth's surface and it bolsters spatial resolution. Then, the purpose of this study is to determine the effect of temperature on actual evapotranspiration using satellite image.

Evapotranspiration occurs from evaporation and transpiration, and it can be obtained from weather data and satellite images. Evaporation is the primary process of water transfer in the hydrological cycle. The water is transformed into vapour and transported into the sky. Evaporation can be classified into potential evaporation and actual evaporation. The potential evaporation is defined as the amount of evaporation that would occur if a sufficient water source were available. On the other hand, the actual evaporation is the amount of water which is evaporated a normal day. The potential evaporation is the maximum value of the actual evaporation. Transpiration is included by the vaporization of liquid water contained in plant tissues and the vapor removal to the atmosphere. (Hongjie et al., 2002; Kalluri et al., 2003) Evapotranspiration is normally computed from the Penman-Monteith FAO 56 equation using weather data. This equation is affected by principal weather parameters such as radiation, air temperature, humidity and wind speed. These parameters can be measured by weather station and computed by the equation of FAO irrigation and Drainage Paper No. 56 (Allen et al., 1998). In addition to the Penman-Monteith FAO 56 equation, evapotranspiration can be estimated from the concept of energy

balance. The main components of the energy balance equation are sensible heat flux, latent heat flux, soil heat flux, and net radiation. These elements relate with incoming and outgoing radiation in the atmosphere, ground surface, and root zone. They are estimated from remote sensing data and weather data. (Wei and Sado, 1994; Amin *et al.*, 1997; Xihua *et al.*, 1997; Andrew *et al.*, 2002)

Remotely sensed data are used for studying the Earth's surface. Current technology allows continuous acquisition of data, regular revisit capabilities (resulting in up-to-date information), broad regional coverage, good spectral resolution (including infra-red bands), good spatial resolution, ability to manipulate/enhance digital data, ability to combine satellite digital data with other digital data, cost-effective data, map-accurate data, possibility of stereo viewing, and large archives of historical data. Remote sensing helps to record data from remote locations. Satellite data provides timely and detailed information about the Earth's surface, especially in relation to the management of our renewable and non-renewable resources. The advantages of satellite data for many fields include for example; assessment and monitoring of vegetation types and their status, soil surveys, mineral exploration, map making and revision, production of thematic maps, water resources planning and monitoring, urban planning, agricultural property planning and management, crop yield assessment, and natural disaster assessment.

The Surface Energy Balance Algorithm for Land or SEBAL (Bastiaanssen *et al.*, 1998a and Bastiaanssen *et al.*, 1998b) is an image processing model to calculate evapotranspiration by using satellite imagery and weather data with the concept of energy balance at the land surface, so evapotranspiration for each pixel is calculated. Satellite images that can be used in SEBAL are LANDSAT, NOAA-AVHRR, MODIS, and ASTER. The advantages of SEBAL are easily applicable because of minimal collateral data needed, applicable to various climates because of physical concepts, no need for land use classification, no need to involve data demanding hydrology, and is a suitable method for all visible, near-infrared and thermal radiometers. However, the disadvantages of SEBAL include cloud-free conditions being required and that surface roughness is poorly described, so that SEBAL is only suitable for flat terrain. (Timmermans *et al.*, 2001; Allen *et al.*, 2001; Lal *et al.*, 2001; Ines, 2002; Abou and Tanton, 2003; Jacob *et al.*, 2003)

2. Landsat 5 TM

Landsat 5 TM has a unique and necessary role in the realm of earth observing satellite orbits, because no other satellite of the earth observing system matches with the synoptic coverage, high spatial resolution, spectral range and radiometric calibration of Landsat's system. Landsat 5 TM satellite imagery Path/Row:127/48 was mainly input data. The spatial resolution of Landsat 5 TM satellite imagery is 30 m and the swath width covered by the image is 185 km. The details of Landsat 5 TM characteristic are shown in Table 1 and Table 2. (Farr, 1999) At the ground stations, the Landsat ground system consists of a spacecraft control center, ground stations for uplinking commands and receiving data, a data handling facility and a data archive, which were developed by the Goddard Space Flight Center, Greenbelt, MD., in conjunction with the U.S. Geological Survey (USGS) EROS Data Center (EDC), Sioux Falls, SD. These facilities will receive, process, archive, and distribute ETM+ data to users. Raw ETM+ data can be transmitted to the EROS Data Center by the ground system within 24 hours of its reception. (Farr, 1999; Liu, 2000; and Liang et al., 2001)

Characteristic	Specification
Swath width:	185 km
Repeat coverage interval:	16 days (233 orbits)
Altitude:	705 km
Quantization:	Best 8 of 9 bits
On-board data storage:	~ 375 Gb (solid state)
Inclination:	Sun-synchronous, 98.2 degrees
Equatorial crossing:	Descending node; 10:00 am +/- 15 min
Launch vehicle:	Delta ll
Launch date:	April 1999

Table 1. Landsat 5 TM mission specification

Channel	Spectral Range (microns)	Ground Resolution (m)
1 (Visible and near infrared: VNIR)	0.450 - 0.515	30
2 (Visible and near infrared: VNIR)	0.525 - 0.605	30
3 (Visible and near infrared: VNIR)	0.630 - 0.690	30
4 (Visible and near infrared: VNIR)	0.750 - 0.900	30
5 (Short wavelength infrared: SWIR)	1.550 - 1.750	30
6 (Thermal long wavelength infrared: LWIR)	10.40 - 12.50	60
7 (Short wavelength infrared: SWIR)	2.090 - 2.350	30
Pan (Visible and near infrared: VNIR)	0.520 - 0.900	15

Table 2. Landsat 5 TM characterist

This Landsat 5 TM image covers Sri Songkhram sub-river basin where locates in the lower part of Mekhong river basin. Mekhong river basin is in the northeast of Thailand. The time period of this study is from November 2006 to January 2007. They were selected because they are in the period of the dry season. Also, They are in the condition of clear sky. Moreover, there is the cultivation during this time so there are both evaporation and transpiration that is evapotranspiration.

3. Radiation

Extraterrestrial radiation (R_a) is the solar radiation received at the top of the earth's atmosphere on a horizontal surface. The values of extraterrestrial radiation depend on seasons change, the position of the sun, and the length of the day. Therefore, the extraterrestrial radiation is a function of latitude, and the date and time of day. The solar constant is the radiation striking a surface perpendicular to the sun's rays at the top of the earth's atmosphere and it is some 0.082 MJ m^{-2} min^{-1}. If the position of the sun is directly overhead, the incidence angle of extraterrestrial radiation is zero. In this case, extraterrestrial radiation is some 0.082 MJ m^{-2} min^{-1}.

Solar or shortwave radiation (R_s) is the amount of radiation penetrating from the atmosphere to a horizontal plane. The sun emits energy by electromagnetic waves that include short wavelengths so solar radiation is referred to as shortwave radiation. In the atmosphere, radiation is absorbed, scattered, or reflected by gases, clouds, and dust. For a cloudless day, the solar radiation is about 75% of the extraterrestrial radiation, while it is

about 25% of the extraterrestrial radiation on a cloudy day. The solar radiation, which is known as global radiation, is a summation of direct shortwave radiation from the sun and a diffuse sky radiation from all upward angles.

Relative shortwave radiation (R_s/R_{so}) is a relationship between shortwave radiation (R_s) and clear-sky solar radiation (R_{so}). The shortwave radiation is solar radiation that actually reaches to the earth's surface in a given time, while clear-sky solar radiation is solar radiation that reaches to the same area with a clear-sky condition. The relative shortwave radiation is affected by the cloudiness of the atmosphere. On a cloudy day, the ratio is smaller than on a cloudless day. The range of this ratio is between 0.33 (cloudy condition) to 1.00 (cloudless condition).

Relative sunshine duration (n/N) shows the cloudiness in the atmosphere. It is the relationship between the actual duration of sunshine (n) and the maximum possible duration of sunshine, or daylight hours (N). For the cloudless condition, n is equal to N, while n and n/N are nearly zero for the cloudy condition. The maximum possible duration of sunshine, or daylight hours (N), depends on the position of the sun, so it is a function of latitude and date. The daily values of N throughout a year differ with latitude.

Albedo (α) is a relationship between reflected radiation and total incoming radiation. It varies with both the characteristics of surface and the angle of incidence, or the slope of ground surface. Albedo can be more than 0.95 for freshly fallen snow, and it is smaller than 0.05 for wet bare soil. The range of albedo for green vegetation is about 0.20 – 0.25 and albedo for the green grass reference crop is 0.23.

Net solar radiation (R_{ns}) is the fraction of the solar radiation that is reflected from the ground surface. It can be calculated by Equation (1):

$$R_{ns} = (1-\alpha)R_s \tag{1}$$

Net longwave radiation (R_{nl}) is the difference in value between outgoing and incoming longwave radiation. The longwave radiation is solar radiation absorbed by the earth and turned to heat energy. Since the temperature of the earth is less than the sun, so the earth emits longer wavelengths. Terrestrial radiation is referred to as longwave radiation. The emitted longwave radiation ($R_{l,up}$) is absorbed by the atmosphere or lost into space. The longwave radiation received by the atmosphere ($R_{l,down}$) increases its temperature. Therefore, the earth's surface both emits and receives longwave radiation. The value of outgoing longwave radiation is normally more than incoming longwave radiation, so the net longwave radiation is used to present the energy loss.

Net radiation (R_n) is the difference in value between incoming and outgoing radiation of both short and long wavelengths. It is the balance among energy absorbed, reflected, and emitted by the earth's surface. The net radiation is also the difference in value between the incoming net shortwave (R_{ns}) and the net outgoing longwave (R_{nl}) radiation. It is a positive value during daytime, while it is a negative value during nighttime. For the total daily value, it is a positive value except for the condition of high latitude.

Soil heat flux (G) is energy that is used in heating the soil. It is a positive value under the condition of warming soil and negative value under the condition of cooling soil. The soil heat flux is very small when compares with net radiation but it cannot be ignored.

4. Temperature calculation

Normally, Landsat 5 TM satellite image data is in the form of Digital Number (DN) so it's necessary to convert from Digital Number to Radiances for all bands in Landsat 5 TM image. An equation for converting is shown in follow equation.

$$L_\lambda = \frac{(LMAX_\lambda - LMIN_\lambda)}{(QCALMAX - QCALMIN)} \times (QCAL - QCALMIN) + LMIN_\lambda \quad (2)$$

where L_λ is spectral radiance at the sensor aperture in watts/(meter squared *ster* μ m), $QCAL$ is the quantized calibrated pixel value in DN, $LMIN_\lambda$ is the spectral radiance that is scaled to $QCALMIN$ in watts/(meter squared *ster* μ m), $LMAX_\lambda$ is the spectral radiance that is scaled to $QCALMAX$ in watts/(meter squared *ster* μ m), $QCALMIN$ is the minimum quantized calibrated pixel value (corresponding to $LMIN_\lambda$) in DN and $QCALMAX$ is the maximum quantized calibrated pixel value (corresponding to $LMAX_\lambda$) in DN.

$LMAX_\lambda$ and $LMIN_\lambda$ are the spectral radiances for each band at digital number 1 and 255 (i.e QCALMIN, QCALMAX), respectively. QCAL or DN, $LMAX_\lambda$ and $LMIN_\lambda$ are input data. These elements are values in header file information.

Thereafter a thermal band or band 6 imagery is converted to the effective at satellite temperature (T_{bb}) calculated by follow equation.

$$T_{bb} = \frac{K_2}{\ln\left(\frac{K_1}{L_6} + 1\right)} \quad (3)$$

For thermal band, calibration constants, K_1 and K_2, are 666.09 watts/(meter squared *ster* μm) and 1282.71 Kelvin, respectively. L_6 is the spectral radiance for band 6 in watts/(meter squared *ster* μm). Then, surface temperature (T_s) is computed by follow equation.

$$T_s = \frac{T_{bb}}{\varepsilon_o^{0.25}} \quad (4)$$

where ε_o is surface emissivity.

5. Actual evapotranspiration calculation

SEBAL is a tool to estimate actual evapotranspiration for flat areas with the most accuracy and confidence. Satellite image and weather data are used in the SEBAL model to calculate actual evapotranspiration by using a surface energy balance at the land surface. SEBAL evaluates an instantaneous actual evapotranspiration flux for the image time, because the satellite image provides information for the overpass time only. The actual evapotranspiration flux can be calculated for each pixel of the image as a residual of the surface energy budget equation. SEBAL needs both shortwave and thermal bands. The required ground-based data is wind speed. The SEBAL energy balance calculates actual evapotranspiration for each pixel for the time of the satellite image, so the results are

instantaneous actual evapotranspiration. To obtain actual evapotranspiration using the conception of SEBAL, following equations are applied (Bastiaanssen et al., 1998a; Bastiaanssen et al., 1998b; Bastiaanssen, 2000; Chemin and Ahmad, 2000; Bastiaanssen *et al.*, 2002).

Firstly, data in the format of radiance is converted to reflectance for all bands. For this converting, thermal band (band 6) is not considered. In practice, band 6 is converted, but it is a dummy in this file. The equation used to convert radiance to reflectance is presented as following.

$$\rho_\lambda = \frac{\pi \times \mathrm{L}_\lambda}{\mathrm{ESUN}_\lambda \times \cos\theta \times \mathrm{d_r}} \tag{5}$$

where ρ_λ is unitless planetary reflectance, L_λ calculates from equation (1), ESUN_λ is mean solar exoatmospheric irradiances from Table 3, θ is solar zenith angle in degrees, and $\mathrm{d_r}$ is the Earth-Sun distance in astronomical that can be obtained from follow equation

$$\mathrm{d_r} = 1 + 0.033\cos\left(\mathrm{DOY}\frac{2\pi}{365}\right) \tag{6}$$

where DOY (or J) is number of day in one year for example DOY of January 1 is 1 while DOY of December 31 is 365.

$$\cos\theta = \cos(90 - \beta) \tag{7}$$

where β is sun elevation angle in degree and $\cos\theta$ is in degree.

$$[\mathrm{Radians}] = \frac{\pi}{180} \times [\mathrm{decimal\ degrees}] \tag{8}$$

Albedo for the top of atmosphere (α_{toa}) can be considered from follow equation

$$\alpha_{\mathrm{toa}} = \sum(\omega_\lambda \times \rho_\lambda) \tag{9}$$

$$\omega_\lambda = \frac{\mathrm{ESUN}_\lambda}{\sum \mathrm{ESUN}_\lambda} \tag{10}$$

where ω_λ is weighting coefficient, which is constant value.

Band	Solar Spectral Irradiances in watts/(meter squared *ster* μm)
1	from 1969 to 1957
2	from 1840 to 1829
3	from 1551 to 1557
4	from 1044 to 1047
5	from 225.7 to 219.3
7	from 82.07 to 74.52
Pan	from 1969 to 1957

Table 3. Solar Spectral Irradiances

Surface albedo equation (α) can be considered from follow equation

$$\alpha = \frac{\alpha_{\text{toa}} - \alpha_{\text{path\_radiance}}}{\tau_{\text{sw}}^2} \tag{11}$$

where α_{toa} is calculated from previous step. $\alpha_{\text{path\_radiance}} \approx 0.03$.

$$\tau_{\text{sw}} = 0.75 + 2 \times 10^{-5} \times z \tag{12}$$

where z is an elevation of area where is defined from Digital Elevation Map (DEM).
Incoming solar radiation ($R_{s\downarrow}$) is estimated in spreadsheet using follow equation.

$$R_{s\downarrow} = G_{sc} \times \cos\theta \times d_r \times \tau_{sw} \tag{13}$$

where G_{sc} is solar constant value, 1367 W/m²
Vegetation indices can be considered from follow equations.

$$\text{NDVI} = \frac{\rho_4 - \rho_3}{\rho_4 + \rho_3} \tag{14}$$

$$\text{SAVI} = \frac{(1+L)(\rho_4 - \rho_3)}{L + \rho_4 + \rho_3} \tag{15}$$

$$\text{LAI} = -\frac{\ln\left(\frac{0.69 - \text{SAVI}}{0.59}\right)}{0.91} \tag{16}$$

where ρ_3 and ρ_4 are reflectance value in red and near-infrared bans (band 3 and 4), respectively. L is constant for SAVI (L= 0.5, when an area have no information for L). L = 0.5 is suitable for this practice.
Surface emissivity (ε_o) can be considered from follow equation

$$\varepsilon_o = 1.009 + 0.047 \times \ln(\text{NDVI}) \tag{17}$$

Outgoing longwave radiation ($R_{L\uparrow}$) can be calculated by following equation

$$R_{L\uparrow} = \varepsilon_o \sigma T_s^4 \tag{18}$$

where σ = 5.67 x 10^{-8} W/(m²-K⁴).
For the selection of "anchor pixel", SEBAL process utilizes two "anchor" pixels to fix boundary condition for the energy balance. (a) "Cold" pixel: a wet, well-irrigated crop surface with full cover ($T_s \cong T_{air}$). In cold pixel, sensible heat flux (H) is usually zero so cold pixel should be selected from water area. (b) "Hot" pixel should be located in a dry and bare agricultural field where one can assume there is no evapotranspiration taking place, and should have a surface albedo similar to other dry and bare field in the area of interest. It should have a LAI in the range of 0 to 0.4. After the temperatures of both cold and hot pixel are defined, these values are used for calculation in the next step.

Incoming longwave radiation ($R_{L\downarrow}$) is computed in spreadsheet using following equation.

$$R_{L\downarrow} = \varepsilon_a \times \sigma \times T_{cold}^4 \tag{19}$$

$$\varepsilon_a = 0.85 \times (-\ln \tau_{sw})^{0.09} \tag{20}$$

where ε_a is an atmospheric emissivity.
Net surface radiation flux (R_n) can be computed by following equation.

$$R_n = R_{s\downarrow} - \alpha R_{s\downarrow} + R_{L\downarrow} - R_{L\uparrow} - (1 - \varepsilon_o) R_{L\downarrow} \tag{21}$$

The soil heat flux (G) can be calculated from following equation.

$$\frac{G}{R_n} = \frac{T_s}{\alpha}\left(0.0038\alpha + 0.0074\alpha^2\right)\left(1 - 0.98\mathrm{NDVI}^4\right) \tag{22}$$

After the above equations are computed, the main equation for sensible heat flux, latent heat flux, evaporative fraction, and 24-hour actual evaporatranspiration are presented as following.
Sensible heat flux (H) is the flux of heat from the earth's surface to the atmosphere. It is not associated with phase changes of water.

$$H = \frac{\rho \times c_p \times dT}{r_{ah}} \tag{23}$$

where ρ is air density (kg/m^3), c_p is air specific heat (1004 J/kg/K), dT (K) is the temperature difference (T_1-T_2) between two heights (z_1 and z_2), and r_{ah} is the aerodynamic resistance to heat transport (s/m).
The estimation of sensible heat flux is the largest drawback, because the temperature difference and aerodynamic resistance to heat transport are unknown for the sensible heat flux calculation. To find these unknowns, SEBAL first calculates the sensible heat flux at extreme dry and wet locations. They are manually identified by the user on the image. The aerodynamic resistance to heat transport is computed from the lower integration constant for r_{ah} (z_1 = 0.1 m.) and the upper integration constant for r_{ah} (z_2 = 2 m.).
For a dry pixel or hot pixel, it should be located in a dry and bare agricultural field where one can be assumed that there is no evapotranspiration taking place. The wet pixel or cold pixel will include a surface temperature equal to air temperature. The sensible heat flux for the cold pixel is usually zero. The linear relationship between the temperature difference (dT) and the surface temperature (T_s), $dT = a + bT_s$, is created, and the coefficients a and b are defined from the two (dT, T_s) pairs applicable to the hot and cold pixels. Then sensible heat flux can be computed for every pixel that has the condition of free convection. Next, the values of friction velocity (u^*) are estimated from the wind speed at the blending height, a value of 200 m will be used. Thereafter, the condition of mixed convection is applied, and the pixel-dependent aerodynamic resistance to heat transfer, r_{ah}, is calculated by using the Monin-Obukhov hypothesis. The new temperature difference is calculated. Finally the processes from the calculation of sensible heat flux to the temperature difference

are repeated until the aerodynamic resistance to heat transfer and temperature difference are stable values. To compute sensible heat flux, following processess are considered.

1. Friction velocity ($u*$) can be computed as follow equation.

$$u* = \frac{ku_x}{\ln\left(\frac{z_x}{z_{om}}\right)} \tag{24}$$

The calculation of the friction velocity requires a wind speed measurement (u_x) at a known height (z_x) in the time of the satellite image. k is a constant (0.41). Then, u_x and z_x are know, but z_{om} is unknown. z_{om} can be calculated in many ways: from z_{om} = 0.12 x height of vegetation (h) for agricultural area, from a land-use map, or from a function of NDVI and surface albedo. At weather station, u_x, z_x, z_{om}, and $u*$ can be determined.

2. Wind speed at a height 200 m above the weather station can be computed as follow equation.

$$u_{200} = \frac{u* \ln\left(\frac{200}{z_{om}}\right)}{k} \tag{25}$$

3. The friction velocity for each pixel is calculated using the wind speed at a height 200 m (u_{200}) that is assumed to be constant for all pixels of the image because it is defined as occurring at a "blending height" unaffected by surface features. From equation (26), z_{om} is unknown to calculate the friction velocity, so z_{om} need to be fined.

$$u* = \frac{ku_{200}}{\ln\left(\frac{200}{z_{om}}\right)} \tag{26}$$

where z_{om} is the particular momentum roughness length of each pixel, z_{om} for each pixel can be computed by two methods: using a land-use map or using NDVI and surface albedo data (z_{om} is calculated in spreadsheet).

For this pattern, a land-use map is not available, and then NDVI and surface albedo data are used. In the method used NDVI and surface albedo, z_{om} is computed from the following equation:

$$z_{om} = \exp\left[\left(a \times \frac{NDVI}{\alpha}\right) + b\right] \tag{27}$$

where a and b are correlation constants derived from a plot of $\ln(z_{om})$ vs $\frac{NDVI}{\alpha}$ for two or more sample pixels representing specific vegetation types. To determine a and b, a series of sample pixels representing vegetation types and conditions of interest are selected and the associated values for NDVI and surface albedo are obtained.

Typical surface albedo values for rice field and deciduous forest are 0.17 – 0.22 and 0.15 – 0.20, respectively.

4. Aerodynamic resistance to heat transport (r_{ah}) is computed as follow equation.

$$r_{ah} = \frac{\ln\left(\frac{z_2}{z_1}\right)}{u * \times k} \tag{28}$$

where z_1 and z_2 are 0.1 m and 2 m, respectively.

5. Near surface temperature difference (dT) for each pixel is calculated using equation (29) and the assumption of a linear relationship between T_s and dT.

$$dT = T_s - T_a \tag{29}$$

where T_a is unknown.

$$dT = b + aT_s \tag{30}$$

where a and b are the correlation coefficients.

To define these coefficients, SEBAL uses the "anchor" pixel where a value for sensible heat flux (H) can be reliably estimated.

a. At the "Cold" pixel

$$H_{cold} = R_n - G - LE_{cold} \tag{31}$$

$$dT_{cold} = \frac{H_{cold} \times r_{ah}}{\rho \times c_p} \tag{32}$$

If "Cold" pixel is chose from a body of water, $H_{cold} = 0$

$$LE_{cold} = R_n - G \tag{33}$$

$$dT_{cold} = 0 \tag{34}$$

b. At the "Hot" pixel

$$H_{hot} = R_n - G - LE_{hot} \tag{35}$$

In the case of H_{hot}, $LE_{hot} = 0$

$$H_{hot} = R_n - G \tag{36}$$

$$dT_{hot} = \frac{H_{hot} \times r_{ah}}{\rho \times c_p} \tag{37}$$

Then, $dT_{cold} = 0$ (T_{cold}, from selection in above step) and $dT_{hot} = \frac{H_{hot} \times r_{ah}}{\rho \times c_p}$ (T_{hot}, from selection in above step)

6. The sensible heat flux is calculated in this step, called initial sensible heat flux.

7. Monin-Obukhov theory in an iterative process is applied in SEBAL to account for the buoyancy effects, which are generated by surface heating. The Monin-Obukhov length (L) is used to define the stability conditions of the atmosphere in the iterative process (this is not the same "L" as used in the SAVI computation). It is a function of the heat and momentum fluxes and is computed as follow:

$$L = -\frac{\rho c_p u*^3 T_s}{kgH} \tag{38}$$

or

$$L = -\frac{1 \times 1004 \times u*^3 T_s}{0.41 \times 9.81 H} \tag{39}$$

8. The values of the stability corrections for momentum and heat transport (ψ_m and ψ_h) are computed as follow. These values depend on the condition of atmosphere.
If L < 0; unstable condition:

$$\psi_{h(200m)} = 2\ln\left(\frac{1+x_{(200m)}}{2}\right) + \ln\left(\frac{1+x_{(200m)}^2}{2}\right) - 2\text{ARCTAN}\left(x_{(200m)}\right) + 0.5\pi \tag{40}$$

$$\psi_{h(2m)} = 2\ln\left(\frac{1+x_{(2m)}^2}{2}\right) \tag{41}$$

$$\psi_{h(0.1m)} = 2\ln\left(\frac{1+x_{(0.1m)}^2}{2}\right) \tag{42}$$

where

$$x_{(200m)} = \left(1 - 16\frac{200}{L}\right)^{0.25} \tag{43}$$

$$x_{(2m)} = \left(1 - 16\frac{2}{L}\right)^{0.25} \tag{44}$$

$$x_{(0.1m)} = \left(1 - 16\frac{0.1}{L}\right)^{0.25} \tag{45}$$

If L > 0; stable condition:

$$\psi_{h(200)} = -5\left(\frac{2}{L}\right) \tag{46}$$

$$\psi_{h(2m)} = -5\left(\frac{2}{L}\right) \tag{47}$$

$$\psi_{h(0.1m)} = -5\left(\frac{0.1}{L}\right) \tag{48}$$

If L = 0; neutral condition: ψ_m and $\psi_h = 0$

9. The friction velocity ($u*$), which is a corrected values, is now computed for each successive iteration as:

$$u* = \frac{u_{200}k}{\ln\left(\frac{200}{z_{om}}\right) - \psi_{m(200m)}} \tag{49}$$

where u_{200} is in m/s and k is 0.41.

10. The aerodynamic resistance to heat transport (r_{ah}), which is a corrected value, is now computed during each iteration as:

$$r_{ah} = \frac{\ln\left(\frac{z_2}{z_1}\right) - \psi_{h(z_2)} + \psi_{h(z_1)}}{u* \times k} \tag{50}$$

11. Repeat the step of calculation from step 5) to 10) until the successive values for dT_{hot} and r_{ah} at the hot pixel have stabilized.

The latent energy of evaporation (LE) was computed using following equation.

$$LE = R_n - G - H \tag{51}$$

After the latent energy of evaporation is computed, the evaporative fraction (Λ) is the next value that is obtained using Equation 52. The evaporative fraction at each pixel of a satellite image can be estimated using the 24-hour evaporatranspiration for the day of the image. The evaporative fraction is assumed to be a constant value over the full 24-hour period.

$$\Lambda = \frac{LE}{R_n - G} = \frac{LE}{LE + H} \tag{52}$$

To estimate 24-hour actual evaporatranspiration, the following equation is utilized.

$$ET_{24} = \frac{86400\Lambda(R_{n24} - G_{24})}{\lambda} \tag{53}$$

where R_{n24} is daily net radiation, G_{24} is daily soil heat flux, 86,400 is the number of seconds in a 24-hour period, and λ is the latent heat of vaporization (J/kg). The 24-hour actual evaporatranspiration, ET_{24}, can be expressed in mm/day.

Since energy, on average, is stored in the soil during the daytime and released into the air at night, G_{24} is very small for the combined vegetative and soil surface, so it can be assumed as zero at the soil surface (Morse et al., 2000). Then, Equation 53 can be rewritten as:

$$ET_{24} = \frac{86400\Lambda R_{n24}}{\lambda} \tag{54}$$

As above equations and calculation process, it can be also presented using Figure 1. Thereafter, to determine the relationship between the temperature and actual evapotranspiration, the maximum and minimum values of actual evapotranspiration in each temperature were ignored. The selected actual evapotranspiration in each temperature was averaged. Finally, the relationship between temperature and actual evapotranspiration was determined using a polynomial equation.

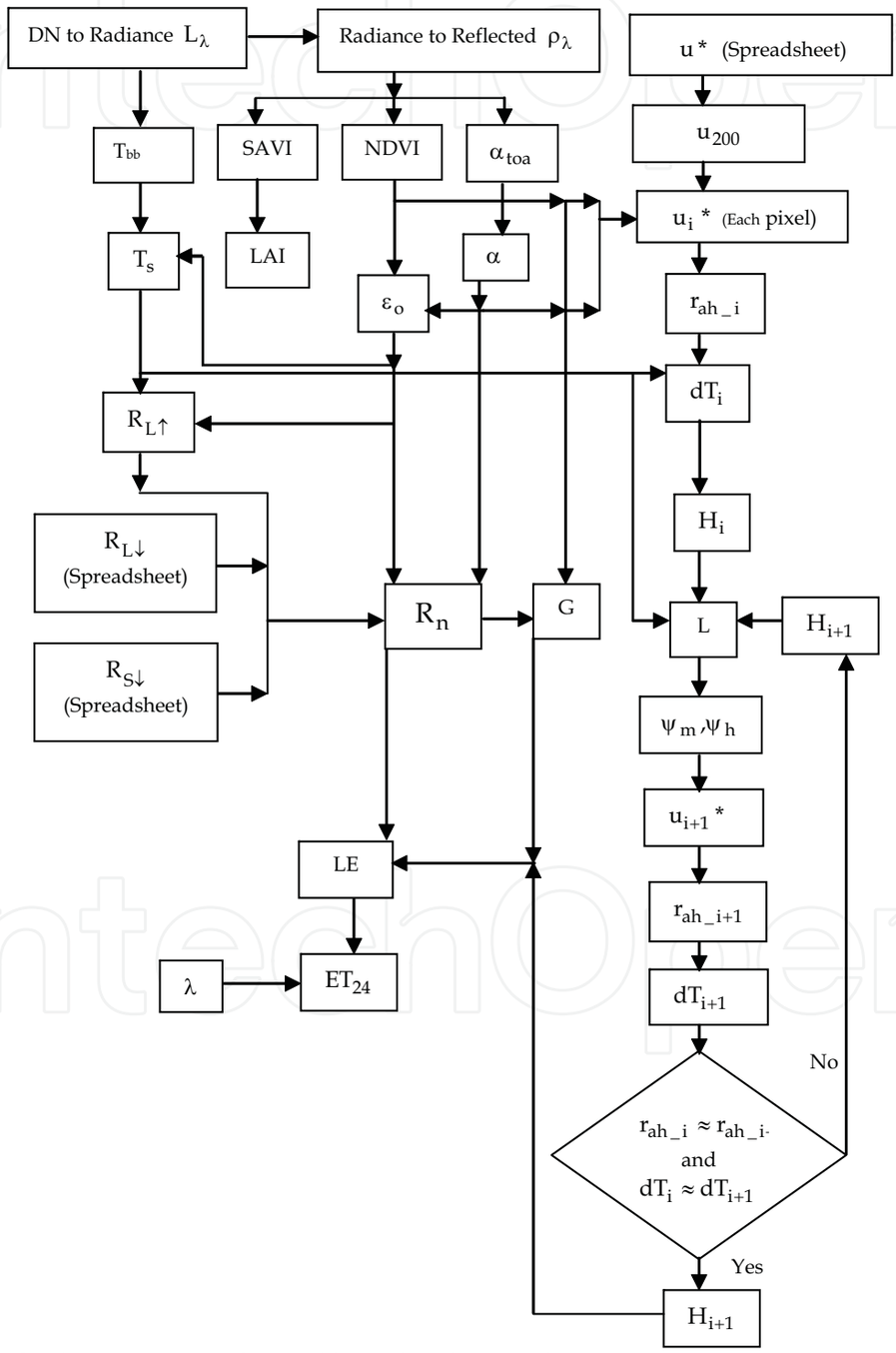

Fig. 1. The Surface Energy Balance Algorithm for Land Process

6. Validation

For the validation of temperature computed by using Landsat satellite image, it was compared with recorded temperature. On the other hand, to validate actual evapotranspiration calculated by SEBAL, recorded pan evaporation was used. Pan evaporation is the amount of water evaporated during a period (mm/day) with an unlimited supply of water (potential evaporation). It is a function of surface and air temperatures, insolation, and wind, all of which affect water-vapor concentrations immediately above the evaporating surface (Chong-yu et al., 2006). On the other hand, actual evapotranspiration is a function of temperature, wind, humidity and net radiation. It can be concluded that there is the relationship between the pan evaporation and actual evapotranspiration. (Humphreys et al., 1994; Grismer et al., 2002; Marco, 2002) Chong-yu et al. (2006) presents that the decreasing trend detected in the pan evaporation and actual evapotranspiration can be attributed to the significant decreasing trends in the net radiation and in the wind speed. Also, it can be attributed to the significant increasing trend in the air temperature.

7. Result

Since there are three main parts for the calculation of this study, there are three main parts of the result that are the spatial temperature, the spatial actual evapotranspiration, and the relation between temperature and actual evapotranspiration. The results for each part are presented as following.

7.1 Spatial temperature

The spatial distributions of temperature calculated by using Landsat 5 TM satellite images are presented from Figure 2 to Figure 4 (Kosa, 2009). These figures can be presented that the mean temperatures from Figure 2 to Figure 4 are 297.34, 295.74 and 296.25 ^{o}K, respectively. On the one hand, the minimum temperatures from these three figures are 283.21, 278.93 and 284.02^{o}K, respectively while the maximum temperatures from these three figures are 308.62, 313.63 and 310.65^{o}K, respectively.

7.2 Spatial actual evapotranspiration

The spatial distributions of actual evapotranspiration calculated by using Landsat 5 TM satellite images and SEBAL are presented from Figure 5 to Figure 7 (Kosa, 2009). These figure cab be presented that the mean actual evapotranspiration from these three figures are 3.67, 4.50 and 4.26mm, respectively.

7.3 Relation between temperature and actual evapotranspiration

After the spatial temperature and spatial actual evapotranspiration were calculated as show in Figure 2 to Figure 7, the temperature and actual evapotranspiration were plotted as present in Figure 8 and 9 (Kosa, 2009). These figures present that equations explained the relation between the temperature and actual evapotranspiration are consisted of $y = -0.028x^2 + 17.069x - 2593.2$ ($R^2 = 0.987$) and $y = -0.028x^2 + 1.7608x - 22.932$ ($R^2 = 0.987$) where y is the actual evapotranspiration (mm/day) and x is the temperature in the unit of ^{0}K and ^{0}C, respectively.

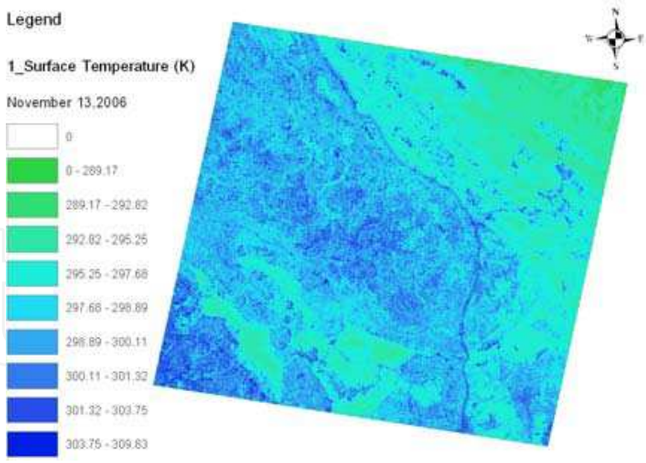

Fig. 2. The surface temperature on November 13, 2006

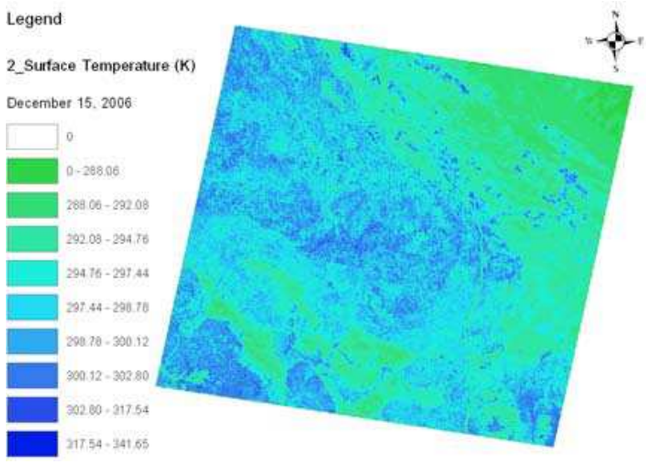

Fig. 3. The surface temperature on December 15, 2006

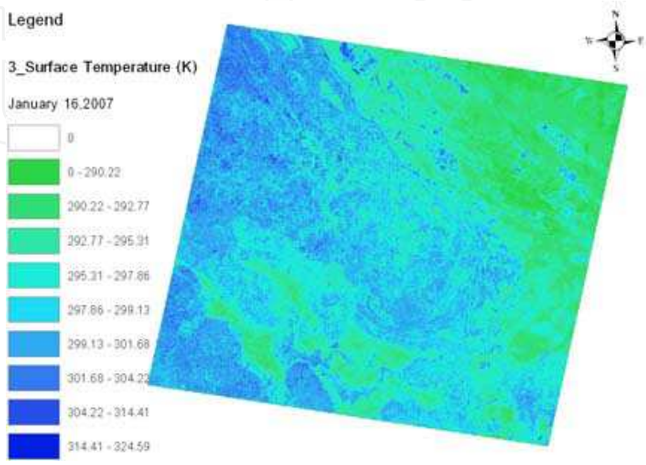

Fig. 4. The surface temperature on January 16, 2007

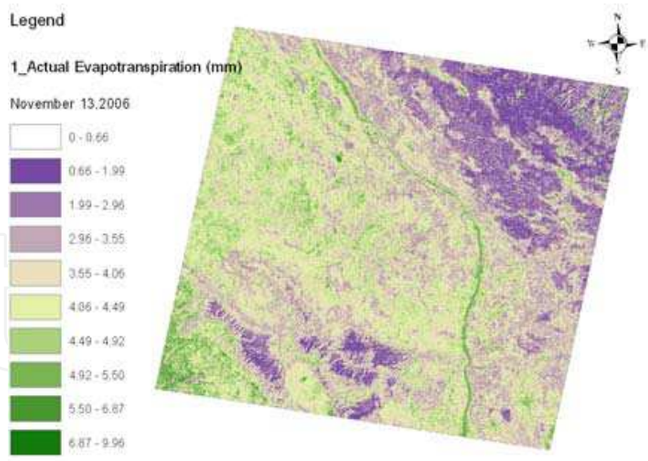

Fig. 5. The actual evapotranspiration on November 13 2006

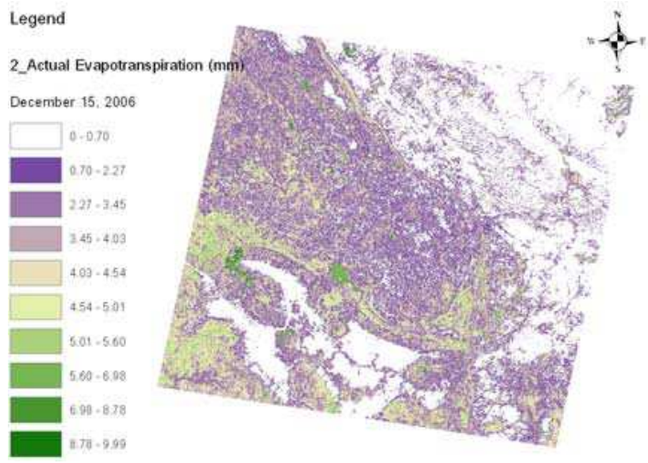

Fig. 6. The actual evapotranspiration on December 15, 2006

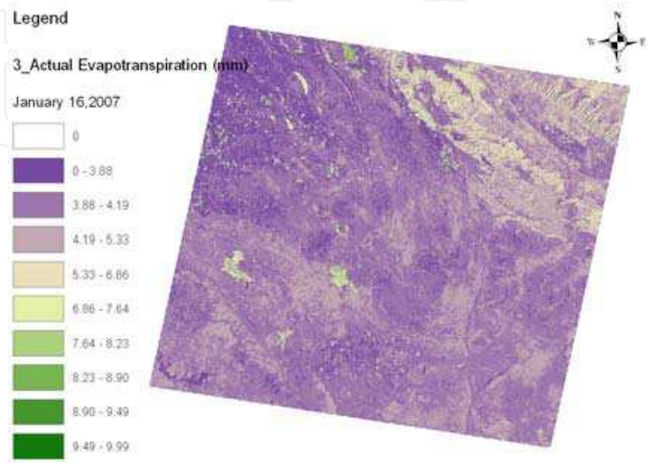

Fig. 7. The actual evapotranspiration on January 16, 2007

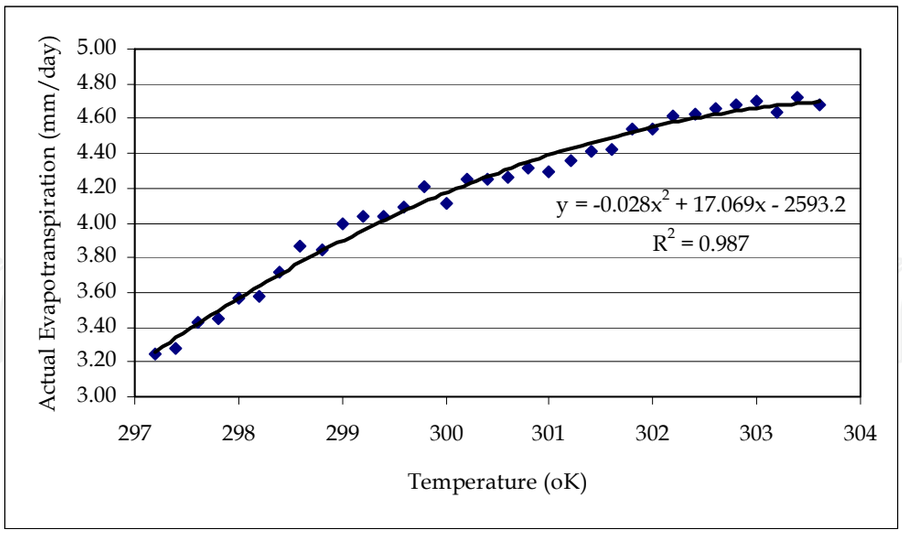

Fig. 8. The relation between the temperature (°K) and actual evapotranspiration (mm/day)

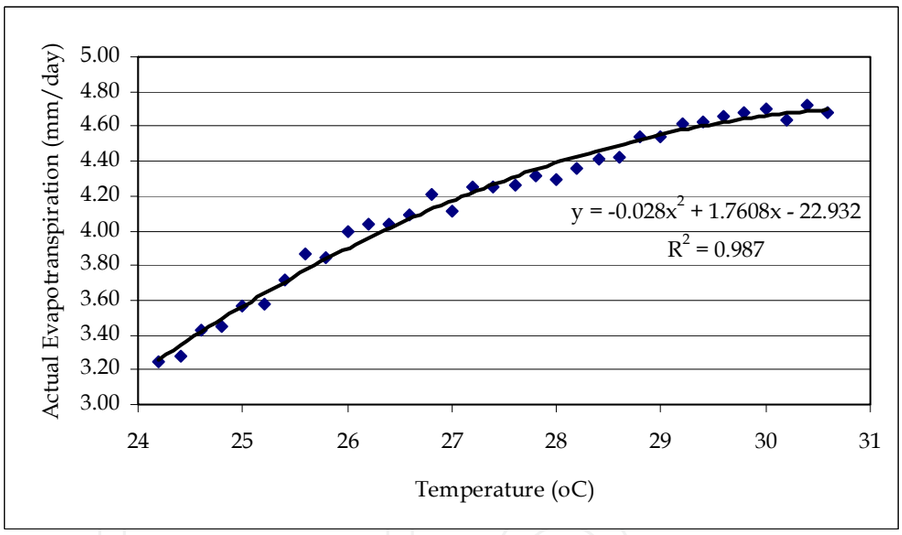

Fig. 9. The relation between the temperature (°C) and actual evapotranspiration (mm/day)

8. Conclusion and recommendation

As above result, it can be concluded that the mean temperature and the mean actual evapotranspiration are 296.44 °K (23.44 °C) and 4.14 mm, respectively. The relationship between the temperature (°K and °C) and actual evapotranspiration (mm/day) is in the format of the polynomial equation. For the temperature in Kelvin, an equation is $y = -0.028x^2 + 17.069x - 2593.2$ and for the temperature in Celsius, an equation is $y = -0.028x^2 + 1.7608x - 22.932$.

The spatial temperature and spatial actual evapotranspiration during November 2006 to January 2007 that are the result are in the condition of both dry season and clear sky. Also, the relationship between temperature and actual evapotranspiration is a result. These

results are useful for irrigation project and water management. For spatial temperature, it presents temperature for each area. Since temperature relates to many weather data, temperature can imply the characteristic of other weather data. For example, high temperature is included low humidity but high evaporation can be occurred in the condition of high temperature. For spatial actual evapotranspiration, it can be used to present daily actual evapotranspiration. This daily actual evapotranspiration leads to the planning of water management in each area. Then, it is easy to manage water by irrigation project. For the relationship between temperature and actual evapotranspiration, it can be used to estimate actual evapotranspiration when temperature is not unknown.

9. Acknowledgements

The authors are grateful to the Suranaree University of Technology for funding, facilities and equipment provided. Satellite images from the Geo-informatics and Space Technology Development Agency (Public Organization) are appreciated.

10. References

Abou E. and T. Tanton. (2003). Real time crop coefficient from SEBAL method for estimating the evapotranspiration, *Proceedings of SPIE*, Vol. 5232.

Allen R.G., Pereira L.S., Dirk R. and Smith M. (1998). Crop evapotranspiration-Guidelines for computing crop water requirements, *FAO Irrigation and drainage paper 56*.

Allen, R. G., A. Morse, M. Tasumi, W. Bastiaanssen, W. Kramber and H. Anderson. (2001). Landsat Thematic Mapper for evapotranspiration via the SEBAL process for water rights management and hydrology water balances, SEBAL, Available Source: http://www.agu.org/meetings/sm01/sm01_pdf/sm01_B42C.pdf, August 8, 2003.

Amin, M. S. M., A. Nabi and S. Mansor. (1997). Use of satellite data to estimate areal evapotranspiration from a tropical watershed, *Asian Conference on Remote Sensing*, 20-24 October 1997, GIS Development Pvt. Ltd., Malaysia.

Andrew, N. F., T. J. Schmugge and W. P. Kustas. (2002). Estimating evapotranspiration over El Reno, Oklahoma with ASTER imagery. *EDP Sciences*, Vol. 22, pp. 105-106.

Bastiaanssen, W. G.M., M. Meneti, R. A. Feddes and A. A. M. Holtslag. (1998a). A remote sensing surface energy balance algorithm for land (SEBAL) 1 Formulation. *Journal of Hydrology*, Vol. 212-213, pp. 198-212.

Bastiaanssen, W. G.M., M. Meneti, R. A. Feddes and A. A. M. Holtslag. (1998b). A remote sensing surface energy balance algorithm for land (SEBAL) 1 Validation. *Journal of Hydrology,* Vol. 212-213, pp. 213-229.

Bastiaanssen, W. G.M. (2000). SEBAL-based sensible and latent heat fluxes in the irrigated Gediz Basin, Turkey. *Journal of Hydrology*, Vol. 229, pp. 87-100.

Bastiaanssen, W. G.M., M. Ahmad and Y. Chemin. (2002). Satellite surveillance of evaporative depletion across the Indus Basin. *Water Resource Research*, Vol. 38, No. 12.

Chemin, Y. and M. Ahmad. (2000). Estimating evaporation using the surface energy balance algorithm for land (SEBAL). *A Manual for NOAA-AVHRR in Pakistan. International Water Management Institute (IWMI)*. Report No. R-102.

Chong-yu XU, Lebing G., Jlang T., and Deliang C. (2006) Decreasing Reference Evapotranspiration in a Warming Climate-A Case of Changjiang (Yangtze) River Catchment During 1970-2000. *Advances Atmospheric Sciences* Vol. 23, pp. 115-131.

Farr, R. (1999). Landsat 7 Project, Policy, and History, Landsat, Available Source: http://landsat.gsfc.nasa.gov/main/project.html, October 21, 2003.

Grismer, M. E., M. Orang, R. Snyder, and R. Matyac (2002). Pan Evaporation to Reference Evapotranspiration Conversion Methods. *Journal of Irrigation and Drainage Engineering*, Vol. 128, No. 3, pp. 180-184.

Hongjie X, Jan H., Shirley K. and Eric S. (2002). Comparison of evapotranspiration estimates from the surface energy balance algorithm (SEBAL) and flux tower data, middle Rio Grande Basin, Evapotranspiration, Available http://www.nmt.edu/~hjxie/sebal-agu.htm, November 29, 2002.

Humphreys, E., W. S. Meyer, S. A. Prathapar and D. J. Smith. (1994). Estimation of evapotranspiration from rice in southern New South Wales: a review. Australian. *Journal of Experimental Agriculture,* Vol. 34, No.7, pp. 1013 – 1020.

Ines A. V. M. (2002). Improved crop production integration GIS and Genetic Algorithm. *Thesis of Doctor Degree*, Asian Institute of Technology, Thailand.

Jacob, F., A. Olioso, X. F. Gu, J. F. Hanocq, O. Hautecoeur and M. Leroy. (2003). Mapping surface fluxes using Visible-Near Infrared and Thermal Infrared data with the SEBAL Algorithm. *Physics and Chemistry of the Earth*.

Kalluri S., Gilruth P., Bergman P. and Plante R. (2003) Impacts of NASA's remote sensing data on policy and decision making at state and local agencies in the United State. Evapotranspiration. Available http://earth-outlook.east.hitc.com:1500/05_07_11.00_kallyri.pdf, August 5, 2003.

Kosa P. (2009) Air Temperature and Actual Evapotranspiration Correlation Using Landsat 5 TM Satellite Imagery. *Kasetsart Journal (Natural Sciences)*, Vol. 43, pp. 605-611.

Lal M., Y. Chemin and L. Chandrapala. (2001). Variability of soil moisture in the Walawe River Basin: A case study in Sri Lanka using low-resolution satellite data, *Asian Comference on Remote Sensing,* 5-9 November 2001. GIS Development Pvt. Ltd., Singapore.

Liang, S., H. Fang and M. Chen. (2001). Atmospheric correction of Landsat ETM+ Land Surface Imagery-Part I: Methods. *IEEE Transactions on Geoscience and Remote Sensing*, Vol. 39, No. 11, pp. 2490-2498.

Liu, J. G. (2000). Evaluation of Landsat-7 ETM+ panchromatic band for image fusion with multispectral bands. *Natural Resources Research*, Vol. 9, No. 4, pp. 269-276.

Marco, A. F. C. (2002). Reference Evapotranspiration Based on Class A Pan Evaporation. *Scientia Agricola Journal,* Vol. 59, No. 3, pp. 417-420.

Morse, A., M. Tasumi, R. G. Allen and J. W. Kramber. (2000). Application of the SEBAL methodology for estimating consumptive use of water and stremflow depletion in the BEAR River Basin of IDAHO through remote sensing. Final Report submit to The Raytheon System Company Earth Obseration System Data and Information System Project.

Timmermans, W. J., A. M. J. Meijerink and M. W. Lubczynski. (2001). Satellite derived actual evapotranspiration and groundwater modeling, Botswana, *Proceedings of a symposium held at Santa Fe, New Mexico, USA*, April 2000. IAHS Publ, No. 267.

Wei, Y. and Sado. K. (1994). Estimation of Areal Evapotranspiration Using Landsat TM data Alone, *Asian Conference on Remote Sensing*, 17-23 November 1994, GIS Development Pvt. Ltd., Bangalore, India.

Xihua, Y., Q. Zhou and M. Melville. (1997). Estimating local sugarcane evapotranspiration using Landsat TM image and a VITT concept. *International Journal of Remote Sensing*, Vol. 18, No. 2, pp. 453-459.

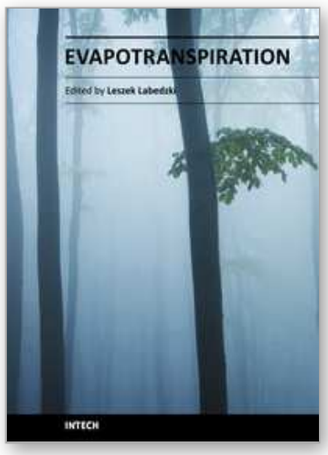

Evapotranspiration

Edited by Prof. Leszek Labedzki

ISBN 978-953-307-251-7
Hard cover, 446 pages
Publisher InTech
Published online 16, March, 2011
Published in print edition March, 2011

Evapotranspiration is a very complex phenomenon, comprising different aspects and processes (hydrological, meteorological, physiological, soil, plant and others). Farmers, agriculture advisers, extension services, hydrologists, agrometeorologists, water management specialists and many others are facing the problem of evapotranspiration. This book is dedicated to further understanding of the evapotranspiration problems, presenting a broad body of experience, by reporting different views of the authors and the results of their studies. It covers aspects from understandings and concepts of evapotranspiration, through methodology of calculating and measuring, to applications in different fields, in which evapotranspiration is an important factor. The book will be of benefit to scientists, engineers and managers involved in problems related to meteorology, climatology, hydrology, geography, agronomy and agricultural water management. We hope they will find useful material in this collection of papers.

InTech Europe
University Campus STeP Ri
Slavka Krautzeka 83/A
51000 Rijeka, Croatia
Phone: +385 (51) 770 447
Fax: +385 (51) 686 166
www.intechopen.com

InTech China
Unit 405, Office Block, Hotel Equatorial Shanghai
No.65, Yan An Road (West), Shanghai, 200040, China
中国上海市延安西路65号上海国际贵都大饭店办公楼405单元
Phone: +86-21-62489820
Fax: +86-21-62489821

IntechOpen